

Intergenerational Cellular Signal Transfer and Erasure

GW C. McElfresh^{*}
J. Christian J. Ray^{†‡}

[‡]To whom correspondence should be addressed.

Biological substrates for computation have been considered since before the advent of modern deterministic computers (McCulloch and Pitts 1943; von Neumann 1956; Bennett 1982). Technological advances in measuring responses of cells to molecular signals have again raised the question of how stochastic networks compute.

Signaling pathways enable living cells to process responses to stimuli from the extracellular environment. The uncertainty of signal transmission in a single cell has prompted various research efforts to quantify how much a cell knows about its environment. Advances in non-equilibrium thermodynamics have arrived alongside analyses of biological signaling. Often, models of signaling that consider only the timescale of molecular fluctuations have been considered (Cheong et al. 2011; Barato, Hartich, and Seifert 2014; Govern and ten Wolde 2014; Bo, Giudice, and Celani 2015; Hartich, Barato, and Seifert 2016, and others), especially in relation to the bacterial chemotactic response (Lan et al. 2012).

^{*}Center for Computational Biology, University of Kansas, USA; gwmcelfresh@ku.edu

[†]Center for Computational Biology and Department of Molecular Biosciences, University of Kansas, USA; jjray@ku.edu

We suggest that an important timescale for biological signaling should be on the order of gene expression (in the case of bacteria, potentially multiple generations). Growing cells invest energy to grow and divide, thereby diluting the results of previous computations. Because the remnants of previous responses are reduced but not necessarily completely erased, gradual dilution imparts a memory effect: a daughter cell is predisposed to respond in a qualitatively similar manner to its mother cell. Quantification of thermodynamic costs of molecular receptor signaling on short timescales is interesting and enlightening about the extreme limits of the biological cost of computation, but such energy use is ultimately minor compared to the massive costs of gene expression that can arise as a result of such a signal. Here we seek to explore the effects of those costs on cellular information processing.

We analyze the effect of cellular memory in a broad class of bacterial information transfer systems, two-component system modules. Two-component systems respond to information about modulation of the physicochemical environment in and around the cell. Our analysis places non-genetic intergenerational information transfer in a computational context and raises the question of the appropriate scales for analyzing the thermodynamics of information in living systems.

Signaling Dynamics on the Timescale of Generations

Two relevant timescales of cellular signaling responses are molecular kinetic fluctuations and the timescale of gene expression programs. In a bacterial cell, the timescale of protein turnover (and thus, shifts in gene expression) is set by the generation time for the majority of protein types. This is because most proteins are quite stable; the relevant quantity for protein kinetic activity is concentration, and growth of the cell is the fastest process that reduces the concentration. Considering a signal that activates a transcription factor, the loss of the signal depends on the elimination of the responding proteins. Thus, for the mean-field birth-death

process with constant production α/τ and constant generation time τ , we have dynamics of protein concentration $x(t)$ as

$$x(t) = e^{-t/\tau} \left(x(0) + \alpha(e^{t/\tau} - 1) \right)$$

and protein half-life after loss of signal is $\tau \ln 2$, or about 70% of a cell lifetime due to growth mediated dilution. Positive feedback on the activation signal can promote the transcriptionally activated state of the cell, further exaggerating the effect. Many studies have explored the implications of such phenotypic memory, e.g. Nevozhay et al. (2012), Kaufmann et al. (2007), Frick et al. (2015), Burrill et al. (2012), Inniss and Silver (2013), Lambert and Kussell (2014), and Ray (2016).

To make the conditions underlying cost and benefit more concrete, we introduce a common signaling pathway in bacteria, the two-component system (TCS). Our goal here is to create a biologically realistic model that allows numerical determination of thermodynamic and informational quantities.

Models of Bacterial Two-Component Signaling

Two-component systems are a common sensing mechanism in bacteria that have a notable level of conservation across phyla (Capra and Laub (2012) review TCS evolution). Though many variations on the core motif exist, the canonical TCS has a dimeric sensor histidine kinase (SHK) and a cognate response regulator (RR). The sensor responds to stimuli by increasing phosphorylated RR (Zschiedrich, Keidel, and Szurmant 2016). Once phosphorylated, RR dimerization is stabilized, allowing it to become a transcription factor for genes that are typically relevant to the original stimulus. In many TCSs one of the operons regulated by the RR is the TCS operon itself, providing feedback and potentially affecting the regulatory activity of the TCS (Batchelor and Goulian 2003; Shin et al. 2006; Shinar et al. 2007; Groban et al. 2009; Ray and Igoshin 2010). TCS operons have strong gene expression polarity, an effect where expression level of the gene closest to the transcription start site is higher

than expression of the subsequent gene(s). Because of this effect, [RR] exceeds [SHK] by orders of magnitude to maintain a sensitive, yet reproducible, response to stimuli (Batchelor and Goulian 2003; Also and Ohki 2003). There are multiple distinct TCSs in most characterized bacterial species, each responding to distinct stimuli and inducing distinct responses (Skerker et al. 2008; Laub and Goulian 2007; Rowland and Deeds 2014). However, TCSs are integrated into global responses. For example, phosphate limitation depends on a complex between multiple sensors, including a TCS sensor called PhoR (Gardner et al. 2014). We developed course-grained models for the TCS core motif that were parameterized to approximately represent a large class of them, but with special reference to the PhoBR system in *Escherichia coli*, which has been extensively studied (Hoffer et al. 2001; Gao and Stock 2013; 2015; 2017, and references therein).

Course-Grained Kinetic Model

The sensor of a TCS is a dimer composed of two inactive monomers. It matures into a dimeric form that is usually in the cell membrane and senses changes in environment. The mature sensor has two reaction pathways: one that favors creating the active regulator, and one that favors the inactivation of the regulator. The result is a dynamic balance between the competing processes of activation and deactivation. Which one dominates at a given time depends on how much stress signal is present. Figure 1a depicts this process. Conformational states in Figure 1a represent ensembles of protein structure conformations that are functionally equivalent in terms of the reaction kinetics, which is why we refer to this as a course-grained kinetic model. All of the depicted reaction rates follow mass action kinetics at this scale.

We have inferred that the SHK component of *E. coli* PhoBR switches between kinase-active and kinase-inactive conformational ensembles because phosphatase activity is unaffected in mutants lacking kinase activity (Carmany, Hollingsworth, and McCleary 2003). Because ATP or ADP

is bound in close proximity to the phosphorylated site on the SHK, the kinase and phosphotransfer reactions are reversible. The step in a TCS that truly dissipates energy is phosphatase activity: effectively irreversible dephosphorylation of a phosphorylated RR monomer.

The cytoplasm contains ATP at ≈ 100 -fold excess over ADP (Qian 2007). Our model assumes that ATP quickly replaces ADP in the binding pocket of SHK molecules. SHK reversibly binds its cognate RR. SHK is then capable of reversibly transferring the phosphoryl group to the RR.

In the limit of large numbers of molecules, the steady state fraction of active SHK is $\frac{k_2}{k_2+k_{-2}}$, and in this model we can say that the rate of kinase phosphorylation is $\frac{k_3 k_2}{k_2+k_{-2}}$. We can find the potential difference (Qian 2007), $\Delta\mu = k_b T \ln \frac{\mathcal{J}^+}{\mathcal{J}^-}$, where \mathcal{J}^+ represents the flux toward transcriptionally active RRP_2 (), \mathcal{J}^- represents the reverse flux, toward the inactive state, and $k_b T$ is the Boltzmann constant times the temperature. In the equilibrium state, the two fluxes balance and we have detailed balance. Deviations of $\Delta\mu$ from zero quantify how far out of equilibrium the system is being driven by mass and energy input from the rest of the cell.

Our TCS model has the following mean-field fluxes:

$$\mathcal{J}^+ = k_1 [SHKm]^2 \times \frac{k_2 k_3}{k_{-2} + k_2} [SHK] \times (k_{-5} + k_4) [SHK.RRP] \times k_6 [RRP]^2$$

$$\mathcal{J}^- = k_{-1} [SHK] \times k_{-3} [SHK.RRP] \times (k_5 + k_{-4}) [RRP] \times k_{-6} [RRP_2]$$

where $[SHKm]$ represents SHK monomers, $[SHK]$ is SHK dimers, $[SHK.RRP]$ is the SHK + RR complex, $[RRP]$ is phosphorylated RR monomer, and $[RRP_2]$ is transcriptionally active, phosphorylated RR dimer. We have identified specific parameter values for each rate constant that reflect the PhoBR system (Table 1).

In practice, living cells constantly produce ATP; the TCS has a constant source of energy in ATP and a sink in $ADP + P_i$. The gene regulatory activity of the TCS, including its autoregulation, also contributes to the total energy in the system. The steady state of a functional TCS is intrinsically out of equilibrium, and at steady state $\Delta\mu > 0$.

Connections to Cellular Physiology

Activation of a TCS upregulates a regulon - the set of genes that are the target of the regulator. The cell pays a metabolic cost for the response, but also benefits from the ameliorative activities of the regulon. For example, in the case of phosphate starvation, the PhoBR TCS induces expression of alkaline phosphatase (*phoA*), recovering phosphorus from phosphate ester. However, the complete regulon of PhoBR consists of approximately 40 upregulated genes; the metabolic cost of expressing it is significant. Lynch and Marinov (2015) give a sense of the scale of a regulon. They estimated absolute the cost per gene to be 10^3 – 10^8 hydrolyzed phosphate bonds in bacteria. This is likely to be the majority of the metabolic cost of TCS activation.

We consider the fraction of the growth budget dedicated to the TCS to be $1 - \phi(\rho) = 1 - \chi \frac{\rho}{\rho_{max}}$ where ρ represents the size of the total regulon, ρ_{max} is the maximal hypothetical induction, and χ is the maximal fraction of the growth budget that the regulon can take. We have defined the “growth budget” somewhat amorphously so that we can use $1 - \phi(\rho)$ as a multiplier to limit growth rate. Then we have a growth multiplier that determines the growth benefit from expressing the TCS regulon, $f(\rho) + f_b$. f_b is the basal growth rate without the benefit of the TCS signal while $f(\rho)$ is the ameliorative contribution of the regulon. We take a linear benefit, $f(\rho) = \alpha \frac{\rho}{\rho_{max}}$, where $\alpha + f_b$ represents the maximal growth rate attainable in a given condition without accounting for TCS regulon cost. The net growth rate accounting for both cost and benefit is then

$$\gamma = (1 - \phi(\rho))(f(\rho) + f_b) = \left(1 - \chi \frac{\rho}{\rho_{max}}\right)\left(\alpha \frac{\rho}{\rho_{max}} + f_b\right). \quad (1)$$

The tradeoff effect naturally arises because this form is quadratic in ρ , with a predicted optimal regulon size at the point where $\frac{\partial \gamma}{\partial \rho} \Big|_{\chi, \alpha, f_b, \rho_{max}} = 0$ which gives $\rho_{opt} = \frac{\rho_{max}(\alpha + f_b \chi)}{2\alpha \chi}$.

The situation is not that simple, however, because both α and f_b depend on the same conditions that determine the activation state of the

TCS, kinetic parameter k_2 . The relationship could potentially take a variety of forms. We estimated the relationship empirically: biomass in a chemostat experiment in an *E. coli* strain that has had the *phoB* gene (response regulator) deleted (Marzan and Shimizu 2011). This strain does not produce the TCS regulon. Its steady state biomass in a chemostat at various levels of phosphate starvation therefore gives f_b for the case of the PhoBR system. The biomass data happen to fit an inverse logistic function with $r^2 > 0.999$. Assuming that TCS activation rate, k_2 , is proportional to the degree of phosphate starvation in PhoBR, we have

$$f_b = \frac{a_{\text{fit}}}{b_{\text{fit}} + e^{-c_{\text{fit}} + k_2}}.$$

$\alpha + f_b$ is the maximum possible recovery from the signal-induced growth rate: with γ_u as the upper limit of the growth rate and ϵ (≤ 1) as the efficiency of the regulon to recover growth rate,

$$\alpha + f_b = \epsilon \left(\gamma_u - \frac{a_{\text{fit}}}{b_{\text{fit}} + e^{k_2 - c_{\text{fit}}}} \right) + \frac{a_{\text{fit}}}{b_{\text{fit}} + e^{k_2 - c_{\text{fit}}}}.$$

For the PhoBR system, we have a growth model with free parameters ϵ , γ_u , χ , and ρ_{\max} . The same study that gave data for the logistic fit of f_b (Marzan and Shimizu 2011) also measured relative expression of selected PhoBR regulon genes in wild-type cultures. From this, we estimated $\chi \approx 0.37$. We assumed that the genes upregulated by the TCS were mostly capable of reducing phosphate stress ($\epsilon = 0.95$), and that the growth medium without phosphate starvation is relatively favorable ($\gamma_u = 0.0004 / \text{s} = 1.44 / \text{h}$). The hypothetical maximum induction of the regulon ($\rho_{\max} = 150 \mu\text{M}$) was set by calibration with the average regulon transcription and translation rates, k_{txnR} and k_{tsnR} (Table 1).

Using the growth model, we created two multiscale models of a TCS embedded in cellular physiology - one representing the average of many cells, and a stochastic simulation that tracks the dynamics of signaling in single cells. We first describe the mean-field model TCS dynamics. We then use this to develop a stochastic model. We calibrate both models

with the mean-field model, explore average responses with it, and then use the stochastic model to simulate the dynamics of signal transfer as the population recovers from signal loss.

Mean-Field Model

We represent two types of processes: reversible chemical reactions, and irreversible reactions that represent dissipative processes such as transcription, translation, cellular growth, and in the TCS, the irreversible step in hydrolysis of ATP—phosphatase activity of SHK. We allowed transcription and translation to be governed by mass-action kinetics. The complete model is a set of differential equations with 12 variables: bicistronic messenger RNA (mRNA), monocistronic RR mRNA, downstream regulon mRNA, downstream regulon protein, and the species represented in Figure 1a.

The equations are omitted for brevity, but all interactions are assumed mass-action except for gene regulation processes, which take Michaelis-Menten form with V_{max} given by k_{txn} (TCS operon) or k_{txnR} (regulon operons) and K_m given by K_{mtxn} (Table 1). (We assume that most promoters of the TCS regulon are calibrated to typical concentrations of RRP₂, and allow the same K_m for the TCS and all regulon promoters). mRNA is unstable and actively degraded by cells; degradation of mRNA is taken to be a mass-action process. Based on Aiso and Ohki (2003), our model has an unstable bicistronic TCS mRNA species capable of initiating translation of both RR and SHK, and a more stable monocistronic mRNA species that only initiates translation of RR. Dilution of molecules depends on the growth model above: loss of protein has a rate $\gamma[\text{Protein}] = (1 - \phi(\rho))(f(\rho) + f_b) \times [\text{Protein}]$ and loss of mRNA has a rate $(k_{degRNA} + \gamma) \times [\text{mRNA}]$ for degradation rate constants that depend on the specific mRNA species.

Stochastic Model

The stochastic model is based on the mean-field model with the following additions. Reactions occur in individual cell agents that have a volume growing according to the growth model described above, based on Bandyopadhyay, Wang, and Ray (2018). Increments of stochastic simulation occur at approximately constant volume intervals, then the volume is updated based on the resulting growth rate. Increments in reaction volume affect any bimolecular interactions (Gillespie 1976). We chose a quasi-constant volume interval of 1 s, which is less than the expected time to add a single phospholipid in a cell that is growing relatively quickly.

For the stochastic growth model, we assume the mean-field growth model holds with the exception of regulon fluctuations. The downstream regulon of a TCS potentially undergoes significant fluctuations that are entrained to RRP₂ fluctuations. However, there is still an independent stochastic component: between the expression of multiple genes, upward fluctuations in some gene expression may be counterbalanced by downward fluctuations in other gene expression. We therefore represented gene expression from $n = 40$ independent loci, all assumed to have identical binding and gene expression kinetics, producing mRNA into a common pool that produces a common regulon.

In the stochastic model, we represent explicit promoters for the regulated genes, with binding/unbinding and irreversible transcription initiation events. We set the binding constants and transcription initiation constants to be equal to the Michaelis-Menten form of the mean-field model (Table 1).

Each cell agent grows at a rate set by the growth model (γ), and when the initial volume has been doubled, it divides, partitioning all non-DNA species into two daughter cells with a binomial distribution. Jun et al. (2018, and references therein) suggest that the “adder” principle is an excellent phenomenological representation of cell volumes during the *E. coli* cell cycle: a constant cell volume is added before division. In our model, each cell agent has a volume of 1 femtoliter and doubles to 2

femtoliters before division. Promoters/DNA are all deterministically inherited into both daughter cells. The cellular simulation is implemented in Python, with the stochastic simulations run in StochKit using GillesPy (Abel et al. 2016) to interface the Python cell script with the stochastic simulations.

Results

Average Cellular Growth and Signal Dynamics

Simulations using the mean field model revealed the effects of induction and shut-off of a TCS in *E. coli* (Figure 2). The model suggests that intermediate levels of induction have a slightly lower growth rate than the fully induced system when the stress becomes more severe (Figure 2c). The reason for the effect is clear looking at the model variants lacking transcriptional feedback with constant low and high TCS gene expression (gray lines in Figure 2). The system with transcriptional feedback switches from being nearly equivalent to the low-TCS-expression feedbackless case to being nearly equivalent to the high-TCS-expression feedbackless case. It is the transcriptional feedback that allows the system to adapt to higher signal levels. Constant high TCS expression causes grossly more ATP hydrolysis (which is the same as the phosphatase flux, $k_{-3} \times ([SHK\alpha.RRP] + [SHK.RRP])$) than the case with low expression or transcriptional feedback (Figure 2d). This demonstrates a tradeoff between cost and benefit: in the autoregulated TCS, it is possible to sacrifice large investments in stress responses, at the cost of slightly lower growth rate unless the stress becomes severe.

Our model predicts that the TCS has a potential difference $\Delta\mu \approx 15 k_b T$, varying slightly depending on signal level (Figure 2b). The same is not true for the ATP dissipation rate of the TCS, which increases dramatically at the largest induction levels (Figure 2d).

We find that shutting off the signal (initial conditions at the $k_2 = 10$ steady state, instantaneously switched to $k_2 = 10^{-3}$) reveals three relevant

timescales (Figure 2e-f). On the generational timescale, $\gg 1000\text{ s}$, the regulon is diluted and normal growth resumes. Loss of TCS transcriptional activity (RRP_2) occurs at a faster rate. At very short timescales, the sensor shuts off to an intermediate quasi-steady state before being driven even lower by the effects of growth dilution (Figure 2f).

Intergenerational Signal Transfer in a Two-Component System

The stochastic cell growth framework captures the rate of signal loss and the interaction between cell division and dynamics of the signal (Figure 3). We used the same switch from high to low signal as above. Figure 3a confirms the mean-field results that signal shutoff is faster than loss of the regulon. Note the half life of RRP_2 being less than half of a generation while the regulon half-life is more than one generation, where a purely growth-diluted molecule half-life would be $\approx 70\%$ of a generation. Both species follow nearly deterministic trajectories. The same is not true for two-component system total protein expression, where protein dilution is highly lineage dependent (Figure 3b). The difference in timescales between the signal shutoff and the residual response illustrates an intergenerational memory effect.

Discussion

It is increasingly feasible to model timescales of cellular information processing that are relevant to fitness and evolution without them being oversimplified toy models. The disadvantage of this approach is the loss of generality: the necessary quantity of empirical information requires that they simulate a specific system. This is a small problem in the face of ever-increasing high-resolution physiological data. The ability to accurately capture interactions between the short timescales of molecular fluctuations and the global physiological shifts in a cell is an unmistakable advantage. Here, we have demonstrated how we can use such models to address questions of energetics and cellular information processing

and have set up a framework for more thorough studies of information flow in the future.

Our model of two-component signaling suggests that the vast majority of metabolic (ATP) cost lies in the production of the regulon, which has a higher ATP investment compared to the signaling system itself. Monte Carlo sampling of the TCS kinetic parameters shows that our empirical parameter set lies in the middle of possible responses (not shown). While it is not precisely quantitative of any particular system, the numerical results are reliable.

In the intact system, the constant source of ATP along with material influx of TCS proteins maintains the TCS out of thermodynamic equilibrium in all conditions (Figure 2b). At the same time, the system is driven by global physiological variables coupled to stochasticity effects, which diversifies the level of memory in a lineage-dependent manner: some cells and all of their daughters undergo rapid loss of TCS proteins while other cells maintain a longer-lived high expression level that may be metastable (Figure 3).

Acknowledgments

This work was supported by the National Institutes of Health award numbers P20GM103418 and P20GM103638. The content is solely the responsibility of the authors and does not necessarily represent the official views of the National Institutes of Health.

Table 1. Calibrated parameters. P_{TCS} refers to the promoter of the two-component system operon.

| Parameter | Estimated Value | Notes/Reference |
|------------------|--------------------------------|--|
| k_1 | $10 (\mu\text{M s})^{-1}$ | Fast SHK dimerization |
| k_{-1} | 0.00001 s^{-1} | Rare SHK de-dimerization |
| k_2 | Conditional, s^{-1} | $k_2 \in [0.001, 10]$ |
| k_{-2} | 0.1 s^{-1} | Assumed fast |
| k_3 | $0.0004 (\mu\text{M s})^{-1}$ | Model calibration |
| k_{-3} | 0.0087 s^{-1} | (Gao and Stock 2013) |
| k_4 & k_{-5} | 1 s^{-1} | Model calibration |
| k_{-4} & k_5 | $0.036 (\mu\text{M s})^{-1}$ | (Gao and Stock 2013) |
| k_6 | $1 (\mu\text{M s})^{-1}$ | Model calibration |
| k_{-6} | 4 s^{-1} | (Mack, Gao, and Stock 2009) |
| k_{txnb} | 0.00001 s^{-1} | Model calibration |
| k_{txn} | 0.00025 s^{-1} | Model calibration |
| k_{txni} | 0.15 s^{-1} | TCS transcription initiation rate when RRP ₂ is bound |
| K_{mtnx} | $2.5 \mu\text{M}$ | P_{TCS} half-sat; (Gao and Stock 2015) |
| k_{pb} | $1.66 (\mu\text{M s})^{-1}$ | P_{TCS} binding rate; (Elf, Li, and Xie 2007) |
| k_{pu} | 3.86 s^{-1} | P_{TCS} unbinding rate; inferred from K_{mtnx} & k_{pb} |
| k_{degb} | 0.027 s^{-1} | (Aiso and Ohki 2003) |
| k_{degr} | 0.0044 s^{-1} | (Aiso and Ohki 2003) |
| k_{tsn} | 0.05 s^{-1} | Model calibration |
| χ | 0.37 | (Marzan and Shimizu 2011) |
| a_{fit} | $\approx 1.123 \times 10^{-4}$ | " |
| b_{fit} | ≈ 1.77 | " |
| c_{fit} | ≈ 3.75 | " |

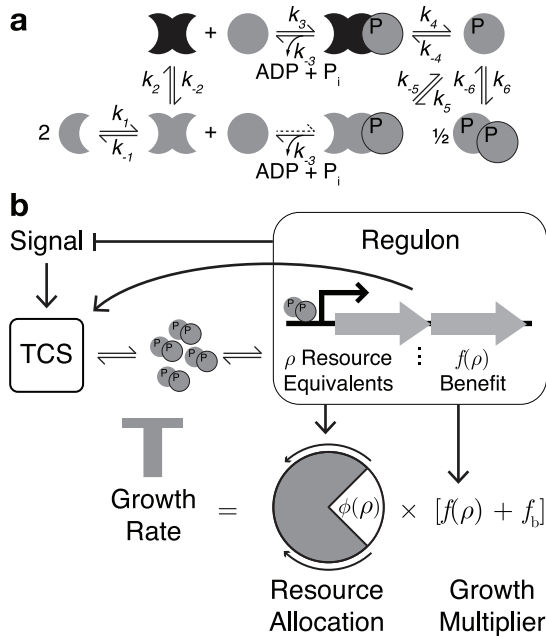


Figure 1. Course-grained multiscale model of a two-component system (TCS). **a.** ATP associates with the sensor histidine kinase (SHK), \blacksquare , along with fast interchange between ADP and ATP. External signal stimulates the SHK conformational switch (k_2). Physical interaction between SHK and response regulator (RR) allows phosphotransfer to RR, stabilizing the dimeric RRP_2 , \bullet^P , an active transcription factor. SHK phosphatase activity is an ATP dissipative step. **b.** Nested feedback loops involved in signals from TCSs. Signal stimulates production of RRP_2 , \bullet^P , which modulates a regulon (upregulation of several genes). Often, transcription of the TCS operon itself is induced: feedback that may affect the signal level. The regulon typically counteracts the signal, another feedback loop. Expression of the regulon entails a metabolic investment, reducing the fraction of resources devoted to growth. Growth dilutes the molecules, affecting bimolecular reaction propensities. The TCS maintains responsiveness by constantly dissipating ATP energy, but the major cost of the TCS during the signal is in the regulon.

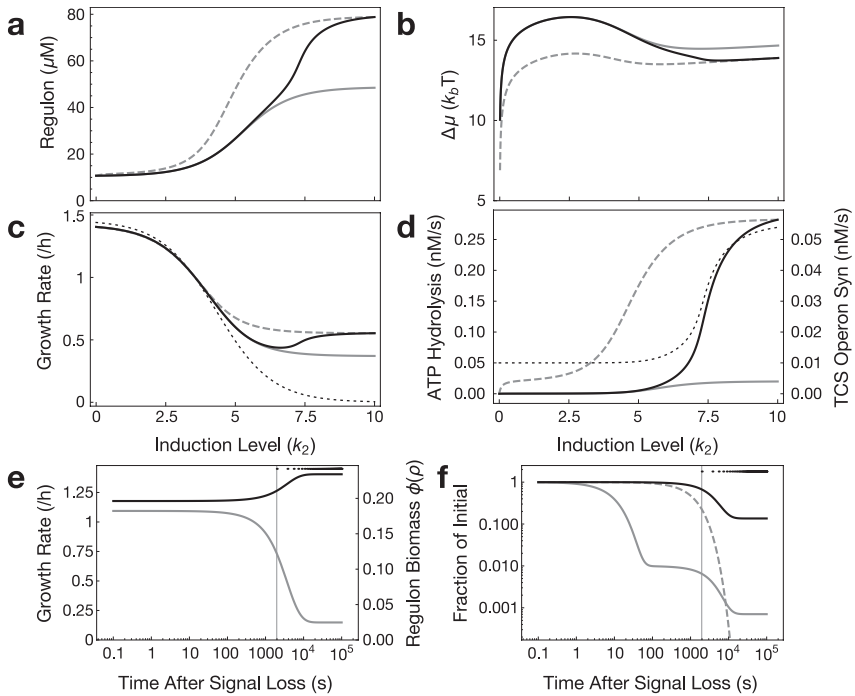


Figure 2. Predicted steady state and dynamical physiological outcomes of activating a two-component system (TCS), with parameters calibrated to represent the *E. coli* PhoBR system having a regulon containing approximately 40 genes. Line styles represent the wild-type system with transcriptional feedback to the phoBR operon (black solid), and transcriptional feedbackless system with basal (gray solid) or maximal (gray dashed) expression. **a.** The level of induction is related to the size of the signal—in this case phosphate limitation. **b.** Potential difference $\Delta\mu$ in units of $k_b T$. **c.** TCS induction recovers a fraction of the growth rate lost to the stress condition. Black dotted line represents the expected growth rate in the absence of the TCS response. **d.** Rates of ATP hydrolysis by the TCS ($k_{-3}([SHK_a.RRP] + [SHK.RRP])$) and TCS operon synthesis ($k_{txnb} + \frac{k_{txnb}[RRP_2]}{K_{m_{txnb}}+[RRP_2]}$). Black dotted line represents the TCS operon synthesis rate. **e.** Dynamics of growth rate and biomass on recovery from fully-induced to uninduced conditions. Black line, growth rate; gray line, biomass. Vertical line: the first generation of growth. Dots represent subsequent generations. **f.** Dynamic loss of TCS activity. Black line, regulon. Gray line, SHKa. Dashed gray, RRP₂.

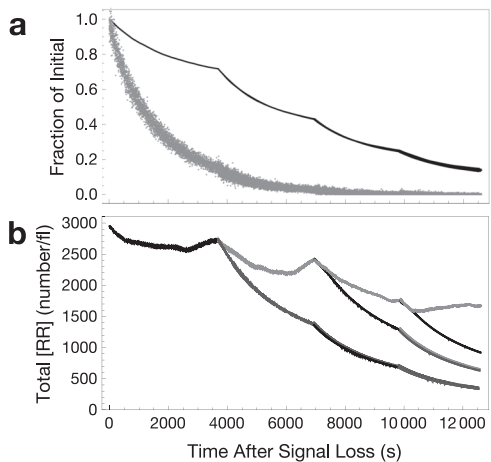


Figure 3. Stochastic dynamics of intergenerational signal loss. The simulation was started in a high activated steady state ($k_2 = 10$) and allowed to relax to an inactive state ($k_2 = 10^{-3}$). **a.** Levels of the two-component system (TCS) regulon (black) and transcriptionally active regulator RRP2 (gray) follow different timescales. Cell division times are evident. These results superimpose the levels in all of the cell agents in the simulation. The results closely follow the expected deterministic mean. **b.** Levels of the two-component system proteins display striking heterogeneity that arises at cell birth. Different individual cells are represented by different shades of gray or black. Some cells are nearly to basal levels of the protein while others still have substantial residual protein several generations later.

References

- Abel, John H, Brian Drawert, Andreas Hellander, and Linda R Petzold. 2016. "GillesPy: A Python Package for Stochastic Model Building and Simulation." *IEEE Life Sciences Letters* 2 (3): 35–38.
- Aiso, Toshiko, and Reiko Ohki. 2003. "Instability of sensory histidine kinase mRNAs in *Escherichia coli*." *Genes to Cells* 8 (2): 179–187.
- Bandyopadhyay, Arnab, Huijing Wang, and J. Christian J. Ray. 2018. "Lineage space and the propensity of bacterial cells to undergo growth transitions." *PLOS Computational Biology*: In press.
- Barato, Andre C., David Hartich, and Udo Seifert. 2014. "Efficiency of cellular information processing." *New Journal of Physics* 16:103024.
- Batchelor, Eric, and Mark Goulian. 2003. "Robustness and the cycle of phosphorylation and dephosphorylation in a two-component regulatory system." *Proceedings of the National Academy of Sciences* 100 (2): 691–696.
- Bennett, Charles H. 1982. "The thermodynamics of computation—a review." *International Journal of Theoretical Physics* 21 (12): 905–940.
- Bo, Stefano, Marco Del Giudice, and Antonio Celani. 2015. "Thermodynamic limits to information harvesting by sensory systems." *Journal of Statistical Mechanics* P01014.
- Burrill, Devin R, Mara C Inniss, Patrick M Boyle, and Pamela A Silver. 2012. "Synthetic memory circuits for tracking human cell fate." *Genes & Development* 26 (13): 1486–1497.
- Capra, Emily J, and Michael T Laub. 2012. "Evolution of two-component signal transduction systems." *Annual Review of Microbiology* 66:325–347.

- Carmany, Daniel O, Kristine Hollingsworth, and William R McCleary. 2003. "Genetic and biochemical studies of phosphatase activity of PhoR." *Journal of Bacteriology* 185 (3): 1112–1115.
- Cheong, Raymond, Alex Rhee, Chiaochun Joanne Wang, Ilya Nemenman, and Andre Levchenko. 2011. "Information transduction capacity of noisy biochemical signaling networks." *Science* 334 (6054): 354–358.
- Elf, Johan, Gene-Wei Li, and X Sunney Xie. 2007. "Probing transcription factor dynamics at the single-molecule level in a living cell." *Science* 316 (5828): 1191–1194.
- Frick, Peter L, Bishal B Paudel, Darren R Tyson, and Vito Quaranta. 2015. "Quantifying heterogeneity and dynamics of clonal fitness in response to perturbation." *Journal of Cellular Physiology* 230 (7): 1403–1412.
- Gao, Rong, and Ann M Stock. 2013. "Probing kinase and phosphatase activities of two-component systems in vivo with concentration-dependent phosphorylation profiling." *Proceedings of the National Academy of Sciences* 110 (2): 672–677.
- . 2017. "Quantitative kinetic analyses of shutting off a two-component system." *MBio* 8 (3): e00412–17.
- . 2015. "Temporal hierarchy of gene expression mediated by transcription factor binding affinity and activation dynamics." *MBio* 6 (3): e00686–15.
- Gardner, Stewart G, Kristine D Johns, Rebecca Tanner, and William R McCleary. 2014. "The PhoU protein from *Escherichia coli* interacts with PhoR, PstB, and metals to form a phosphate-signaling complex at the membrane." *Journal of Bacteriology* 196 (9): 1741–1752.
- Gillespie, Daniel T. 1976. "A general method for numerically simulating the stochastic time evolution of coupled chemical reactions." *Journal of Computational Physics* 22 (4): 403–434.

- Govern, Christopher C., and Pieter Rein ten Wolde. 2014. “Optimal resource allocation in cellular sensing systems.” *Proceedings of the National Academy of Sciences* 111 (49): 17486–17491.
- Groban, Eli S, Elizabeth J Clarke, Howard M Salis, Susan M Miller, and Christopher A Voigt. 2009. “Kinetic buffering of cross talk between bacterial two-component sensors.” *Journal of Molecular Biology* 390 (3): 380–393.
- Hartich, David, Andre C. Barato, and Udo Seifert. 2016. “Sensory capacity: An information theoretical measure of the performance of a sensor.” *Physical Review E* 93:022116.
- Hoffer, Sally M, Hans V Westerhoff, Klaas J Hellingwerf, Pieter W Postma, and Jan Tommassen. 2001. “Autoamplification of a two-component regulatory system results in “learning” behavior.” *Journal of Bacteriology* 183 (16): 4914–4917.
- Inniss, Mara C, and Pamela A Silver. 2013. “Building synthetic memory.” *Current Biology* 23 (17): R812–R816.
- Jun, Suckjoon, Fangwei Si, Rami Pugatch, and Matthew Scott. 2018. “Fundamental Principles in Bacterial Physiology-History, Recent progress, and the Future with Focus on Cell Size Control: A Review.” *Reports on Progress in Physics* 81:056601.
- Kaufmann, Benjamin B, Qiong Yang, Jerome T Mettetal, and Alexander van Oudenaarden. 2007. “Heritable stochastic switching revealed by single-cell genealogy.” *PLOS Biology* 5 (9): e239.
- Lambert, Guillaume, and Edo Kussell. 2014. “Memory and fitness optimization of bacteria under fluctuating environments.” *PLOS Genetics* 10 (9): e1004556.
- Lan, Ganhui, Pablo Sartori, Silke Neumann, Victor Sourjik, and Yuhai Tu. 2012. “The energy–speed–accuracy trade-off in sensory adaptation.” *Nature Physics* 8:422–428.

- Laub, Michael T, and Mark Goulian. 2007. "Specificity in two-component signal transduction pathways." *Annual Review of Genetics* 41:121–145.
- Lynch, Michael, and Georgi K Marinov. 2015. "The bioenergetic costs of a gene." *Proceedings of the National Academy of Sciences* 112 (51): 15690–15695.
- Mack, Timothy R, Rong Gao, and Ann M Stock. 2009. "Probing the roles of the two different dimers mediated by the receiver domain of the response regulator PhoB." *Journal of Molecular Biology* 389 (2): 349–364.
- Marzan, Lolo Wal, and Kazuyuki Shimizu. 2011. "Metabolic regulation of *Escherichia coli* and its *phoB* and *phoR* genes knockout mutants under phosphate and nitrogen limitations as well as at acidic condition." *Microbial Cell Factories* 10 (1): 39.
- McCulloch, Warren S, and Walter Pitts. 1943. "A logical calculus of the ideas immanent in nervous activity." *Bulletin of Mathematical Biophysics* 5 (4): 115–133.
- Nevozhay, Dmitry, Rhys M Adams, Elizabeth Van Itallie, Matthew R Bennett, and Gábor Balázsi. 2012. "Mapping the environmental fitness landscape of a synthetic gene circuit." *PLOS Computational Biology* 8 (4): e1002480.
- Qian, Hong. 2007. "Phosphorylation Energy Hypothesis: Open Chemical Systems and Their Biological Functions." *Annual Review of Physical Chemistry* 58:113–142.
- Ray, J Christian J. 2016. "Survival of phenotypic information during cellular growth transitions." *ACS Synthetic Biology* 5 (8): 810–816.
- Ray, J Christian J, and Oleg A Igoshin. 2010. "Adaptable functionality of transcriptional feedback in bacterial two-component systems." *PLOS Computational Biology* 6 (2): e1000676.

- Rowland, Michael A, and Eric J Deeds. 2014. "Crosstalk and the evolution of specificity in two-component signaling." *Proceedings of the National Academy of Sciences* 111 (15): 5550–5555.
- Shin, Dongwoo, Eun-Jin Lee, Henry Huang, and Eduardo A Groisman. 2006. "A positive feedback loop promotes transcription surge that jump-starts *Salmonella* virulence circuit." *Science* 314 (5805): 1607–1609.
- Shinar, Guy, Ron Milo, María Rodríguez Martínez, and Uri Alon. 2007. "Input–output robustness in simple bacterial signaling systems." *Proceedings of the National Academy of Sciences* 104 (50): 19931–19935.
- Skerker, Jeffrey M, Barrett S Perchuk, Albert Siryaporn, Emma A Lubin, Orr Ashenberger, Mark Goulian, and Michael T Laub. 2008. "Rewiring the specificity of two-component signal transduction systems." *Cell* 133 (6): 1043–1054.
- von Neumann, John. 1956. "Probabilistic logics and the synthesis of reliable organisms from unreliable components." *Automata Studies* 34:43–98.
- Zschiedrich, Christopher P, Victoria Keidel, and Hendrik Szurmant. 2016. "Molecular mechanisms of two-component signal transduction." *Journal of Molecular Biology* 428 (19): 3752–3775.